Deep and machine learning methods for the (semi-)automatic extraction of sandy shoreline and erosion risk assessment basing on remote sensing data (case of Jerba island -Tunisia)

Amina Boussetta, Simona Niculescu, Soumia Bengoufa, Mohamed Faouzi Zagrarni

To cite this version:

Amina Boussetta, Simona Niculescu, Soumia Bengoufa, Mohamed Faouzi Zagrarni. Deep and machine learning methods for the (semi-)automatic extraction of sandy shoreline and erosion risk assessment basing on remote sensing data (case of Jerba island -Tunisia). Remote Sensing Applications: Society and Environment, 2023, 32, pp.101084. 10.1016/j.rsase.2023.101084 . hal-04281261

HAL Id: hal-04281261
https://hal.science/hal-04281261

Submitted on 27 Nov 2023

Deep and machine learning methods for the (semi-)automatic extraction of sandy shoreline and erosion risk assessment basing on remote sensing data (case of Jerba Island -Tunisia)

Amina Boussetta[a,*],Simona Niculescu[b, c], Soumia Bengoufa [b], Mohamed Faouzi Zagrarni[a]

[a]U.R Applied Hydrosciences UR13ES81, Institut Supérieur des Sciences et Techniques des Eaux de Gabès (ISSTEG), University of Gabès, Tunisia

[b]Univ Brest, CNRS, Nantes Université, Université de Rennes, LETG, UMR 6554, F-29280 Plouzané, France

[c] Institut universitaire de France (IUF)

Abstract

Against the backdrop of the environmental crisis, the socio-economic, ecological and cultural importance of the coastal zone calls for greater awareness of how coastal resources function, evolve, are managed and enhanced. This study aims to develop a high-performance (semi-)automatic coastal monitoring method based on Landsat-5 and Sentinel-2 multispectral satellite images for spatiotemporal analysis of shoreline changes and erosion risk assessment along Jerba Island (Tunisia) using remote sensing data and geospatial tools. A comparative study between the band ratioing (BR) method and the pixel-based image analysis (PBIA) and object-based image analysis (OBIA) methods has led to the development of machine learning (ML), random forest (RF), deep learning (DL) and convolutional neural network (CNN) algorithms. Using these classification methods, 15 different shorelines were successively detected in 1989, 2015 and 2023 and then compared with a digitized reference shoreline from the Landsat-5 and Sentinel-2 images. Following a quantitative evaluation, the accuracy of the classification model shows that the combined CNN-OBIA approach provided the least accurate results, with an overall accuracy (OA) index of 67%, while the OBIA-RF classification method provided the most accurate results (OA of 95%). This comparative study identified an accurate and improved extraction method for quantifying changes in the position of the shoreline on the east coast of Jerba Island, enabling managers to make better decisions on coastal protection and adaptation to climate change.

Keywords: Machine learning; deep learning, erosion, Landsat-TM, Sentinel-2.

1. Introduction

Coastal zones are highly dynamic environments in a perpetual evolution of their natural and anthropogenic origins, generated directly or indirectly by human interventions (Yan, 2023). Factors such as winds, waves, tides, storms or sea-level variations can influence them. In response to these variations, the coastal fringe undergoes temporal and spatial changes (Zagórski et *al.,* 2020). It is generally perceived as either a form of erosion or an accumulation of sediments (Paskoff, 1984). Erosion is thus a natural process that has always shaped the morphology of the coastal fringe and leads to a net change in the sediment budget. The main natural factors for this loss of sediment budget are a combination of material scarcity since the end of the post-glacial transgression, hydrometeorological conditions and sea-level rise (Sanlaville, 2001).

Most sandy shorelines in coastal areas are eroding, which is a cause for great concern. A study of satellite shoreline data by Luijendijk et *al.,* (2018) for the 33-year period from 1984 to 2016 indicates that 24% of the world’s sandy beaches are eroding at a rate of more than 0.5 m per year, while 28% are accreting and 48% are stable. According to studies carried out by Serbaji et *al.,* (2023) on erosion modeling, Tunisia presents a severe risk of coastal erosion, showing that 6.43% of the country's total surface area is affected by a very high rate of erosion, estimated at over 30 t/ha/year, and that 4.20% faces high average rates of erosion, ranging from 20 to 30 t/ha/year. In particular, the most eroded areas were identified in the south-west, center and west of the country. At the regional level, the sandy coasts of Jerba Island in the Gulf of Gabès in southeastern Tunisia are among the areas most affected by erosion. Boussetta et *al.,* (2022a) recently confirmed this erosion trend, with values ranging from -2.87 to -8.42 m/year between 1989 and 2021.

The shoreline is considered the boundary between land and a water surface (Boak and Turner, 2005; Guariglia et *al.*, 2006; Sunder et *al.*, 2017). Shoreline monitoring needs to take into account the spatiotemporal elements underlying the dynamic evolution of the boundary between land and water. In order to estimate erosion rates, the precise extraction of the shoreline remains a difficult task. Various methods have been used to extract and monitor shoreline evolution (Ramesh and Singh, 2020). The most commonly used are manual identification through visual interpretation (Zhao et *al.*, 2022), the thresholding approach (Aedla et *al.*, 2015; McAllister et *al.*, 2022; Toure et *al.*, 2019), airborne LiDAR (Wang et *al.*, 2023), band ratios (Boussetta et *al.*, 2022a; Görmüş et *al.*, 2021) and image classification; supervised and unsupervised (Islam et *al.*, 2021; Souto-Ceccon et *al.*, 2023; Yang et *al.*, 2022).

Over the past decade, approaches to monitoring coastal erosion and shoreline evolution have focused on the spatiotemporal analysis of satellite images. The current trend is towards developing ML and artificial intelligence techniques, such as the CNN model, which can support automated shoreline extraction (Görmüş et *al.,* 2021; Tsiakos and Chalkias, 2023).

ML and DL algorithms, such as neural networks and random forests (RF), have recently been successfully adopted for remote sensing applications (Bengoufa et *al.,* 2021a; Dang et *al.,* 2022; Erdem et *al.,* 2021; Niculescu et *al.,* 2018; Seale et *al.,* 2022), and have the potential to improve our understanding of coastline evolution (Gomez-de la Pena et *al.,* 2023). However, limited research has focused on tasks related to shoreline detection, mainly due to the various morphological features of the shoreline that need to be considered, especially in large-scale monitoring scenarios (Seale et *al.,* 2022). Furthermore, Toure et *al.,* (2019) claimed that the relevance of these methods for shoreline detection had not been sufficiently investigated, and a limited number of studies have assessed the accuracy of these classification approaches based on various new algorithms. Recently, Tsiakos and Chalkias (2023) have argued that using neural networks and deep learning (DL) approaches should be expanded as they can support different land and water segmentation models and coastal zone classification.

Bengoufa et *al.,* (2021a) studied the contribution of several ML algorithms and their accuracy in detecting the shoreline of Mostaganem (Algeria). This research focused on a small section of the coastline and used very high-resolution images (Pleiades), which produced very good results. However, these very high-resolution images are costly and difficult to obtain for third-world countries that need an open source of data to effectively monitor the environmental status of their coastlines. In addition, their research did not include an estimation of the erosion rate, which is the main reason for the shoreline extraction process. We have proposed this research paper to overcome these limitations and as an update and improvement to the work of Bengoufa et *al.,* (2021a) in another complex geographical area using open-source data.

In this context, this study aims to highlight and facilitate the understanding of different approaches based on deep and shallow (semi-)automatic learning applied to coastal erosion and shoreline change monitoring using 1989, 2015 and 2023 medium- and high-resolution multispectral optical images, and in particular open access images (Landsat-5 TM and Sentinel-2 MSI), providing details on their performance, strengths and weaknesses.

Therefore, this study focused on algorithmic development by comparing the effectiveness of the RF algorithm, which is considered a powerful ensemble training technique (Demir et *al.,* 2017; Millard and Richardson, 2015; Rodriguez-Galiano et *al.,* 2012); and the CNN, which is theoretically superior to DL algorithms, and has been successful in classifying remote sensing images (Zhu et *al.,* 2017). Furthermore, this contribution aims to show the potential of OBIA classification method in predicting shoreline evolution, and therefore, a more exhaustive search of parameters could be useful to find the best performing ML model on the study site.

This study allows conclusions to be drawn from new perspectives on multitemporal and multisensory satellite imagery processing. It thus presents a detailed long-term analysis of the evolution of the shoreline of the east coast of Jerba Island with very high accuracy, and validated mainly by in situ observations.

2. Study area

Jerba, located in southeastern Tunisia at northern latitude between 33°57’0.56” and 33°37’46.82” and an eastern longitude between 10°45’38.43” and 11°3’53.802”, is considered the largest island in North Africa. The choice of our study site was based on its ecological importance. It hosts three wetlands of international importance listed by the Ramsar Convention on 7 November 2007, namely the Rass Rmel site, which was the subject of our study. It is the region’s leading tourist destination thanks to its beautiful sandy beaches on the east coast (Figure 1).

Jerba is part of the Mediterranean Gulf of Gabès and is characterized by a microtidal regime, with the most frequent tidal range on the coast being about 0.2 m for neap tides and 1.1 m for spring tides. Geographically, the region is characterized by low-lying land with an average topography of 20m and a gentle slope between 0° and 2.29°. The low topography extends into the submarine zone, with an extensive shallow continental shelf with a -10m isobath averaging 3km from the shore. The low-lying shoreline of the eastern parts of Jerba is characterized by very fine sediments and sandy beaches, which are most affected by changes in shoreline configuration. These characteristics make the island highly vulnerable to coastal erosion.

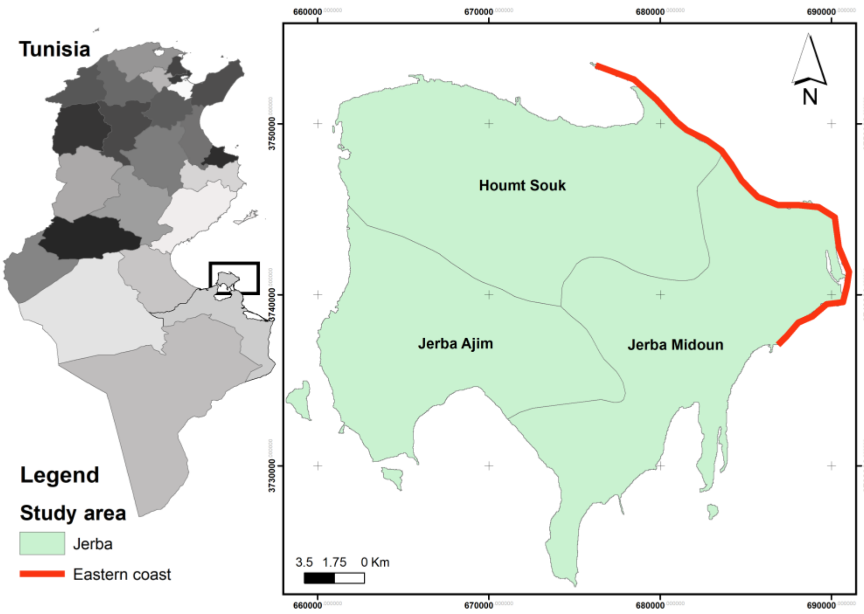

Fig. 1. Jerba Island, south-east Tunisia, selected as the study area

3. Material and methods

The first step of our approach was to analyze the geographical and geomorphological context of the study area through environmental analysis. In 2018, several field surveys were carried out at different times, which allowed us to observe the different signs of coastal erosion and visualize the morphological changes along the shoreline. This analysis identified the land-water boundary for its usefulness and reliability.

Secondly, this study aims to assess the methodological contribution of these approaches to (semi-)automatic shoreline extraction. Thus, a comparative study between four (semi-)automatic methods of band ratioing (BR) and supervised classification, namely, pixel-based image classification (PBIA), object-based image analysis (OBIA), an integrated CNN-OBIA approach and manual digitization.

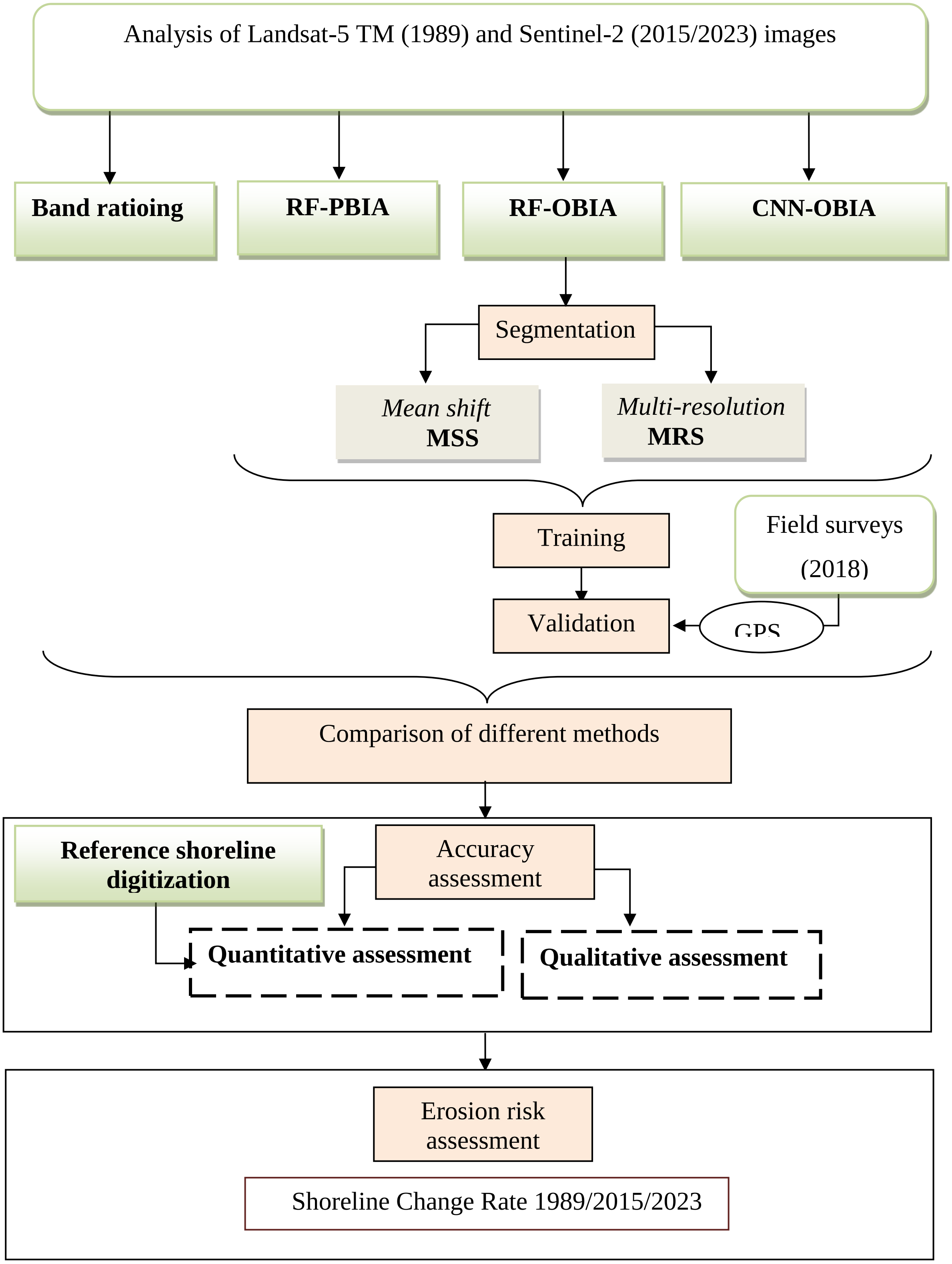

Fig. 2. Flow chart of the comparative study between different classification methods and machine learning algorithms using multi-resolution, multisensor images.

3.1.Data Acquisition

The determination of shorelines using satellite images from a wide range of satellites, including Landsat (Wicaksono and Wicaksono, 2019) and Sentinel (Abdelhady et *al.*, 2022), is becoming increasingly common due to improvements in image resolution, acquisition rates and availability. A Landsat Thematic Mapper (TM) image with a resolution of 30m was used for the year 1989. This was downloaded for free in GeoTIFF format from the United States Geological Survey (USGS) Earth Explorer portal (http://www.earthexplorer.usgs.org). Two high-resolution Sentinel-2 images with a MultiSpectral Instrument (MSI) sensor and 2A processing level were downloaded via the CNES Theia platform (free access; Muscate - Distribution Workshop) with 13 spectral bands of different spatial resolutions ranging from 10 to 60 m. Bands B2, B3, B4 and B8 have a resolution of 10 m. Bands B5, B6, B7 and B8 have a resolution of 20 m, while bands B1, B9 and B10 have a spatial resolution of 60 m.

The Sentinel-2 mission provides an alternative source of optical remote sensing that is globally covered and freely accessible (Wang et *al.*, 2018). High spatial resolution (10 m) data from the Sentinel-2 satellite is mainly used for mapping coastal areas. For the present work, images with the ‘flat reflectance’ band were selected. In this case, the Sentinel images are corrected for slope effects, and all the satellite images used had zero cloud cover.

Table 1. Satellite images used

Acquisition date	Acquisition time	Satellite and sensor	Resolution (m)	Bands used(µm)
07 January 1989	09:19:53	Landsat-5 TM	30*30	B1: 0,45 - 0,52 (Blue) B2: 0,52 - 0,6 (Green) B3: 0,63 - 0,69 (Red) B5: 1,55 - 1,75 (Mid-Infrared)
08 December 2015	10:20:05	Sentinel-2A MSI	10*10	B2=Blue B3=Green B4=Red B8=Near-infrared
10 January 2023	10:11:24	Sentinel-2A MSI		

3.2. Preprocessing

The preprocessing of the Landsat-5 TM scene begins with radiometric correction, where the pixel values refer to the same physical units. As a preprocessing tool, QGIS 3.10 provides the Semi-Automatic Classification plugin, which ensures a one-step attenuation of atmospheric effects, compensation for differences in shooting conditions and sensor calibration. The next step is geometric correction, which uses ground control points (GCPs). Using a global positioning system (GPS), more than 30 well-distributed bitter points were carefully identified in situ at permanent landmarks.

The *flat reflectance* bands of the Sentinel-2 images were already corrected and then further corrected for terrain slope. Using European Space Agency's Sentinel Applications Platform software (SNAP), a subset of four bands (B2/B3/B4/B8) was created.

3.3.Shoreline detection and extraction using machine learning methods (random forest algorithm)

The principle of supervised classification with ML methods is to assign a class to each point selected from a set of possible classes. The data set (pixel or object) must be grouped into several subsets to create classes. This grouping is done based on similarity criteria. A comparative study (Figure 2) assessed the suitability of supervised image classification methods, namely PBIA and OBIA, as well as ML and DL algorithms for shoreline detection and extraction.

3.3.1. Sampling process

It is necessary to have a good knowledge of land use to instruct the treatment system. For this, we need ground-truth data. Ground truth is a guaranteed set of exact data on observed land use obtained through close observations in the field. Furthermore, the selection of samples is always based on very high-resolution Google Earth images with the same dates as the satellite images.

On this basis, certain regions of interest (ROI) were defined to highlight the land-water boundary. The classes are as follows: for the Sentinel image: (1) water, (2) land, (3) urban and (4) vegetation; for the Landsat image: (1) water, (2) land, (3) vegetation and (4) other. The water class represents shallow coastal waters. The land class represents a beach consisting of homogeneous sandy material. The boundary between this class and the water is maintained as the target fault to be extracted, the shoreline.

The sampling step is essential for supervised classification, either for OBIA or PBIA. Indeed, good classification requires representative and suitable samples (Sabat-Tomala et *al.*, 2020). A training sample is necessary for training and developing classification models. The sampling technique consists of taking the number of classes in each sample, making it possible to deal with class imbalance (Sertel et *al.*, 2022). The validation step of the model was done using ground-truth points (validation samples) collected in situ using the GPS. This step is crucial for assessing the accuracy of the assisted classification and capturing the accuracy metrics (see the accuracy assessment section 4.1.4.1).

The training and validation samples (about 850 samples) must be selected in areas highly representative of the objects on Landsat-5 for 1989 and Sentinel-2 images for 2015 and 2023; these areas should be highly reflective to compensate for possible confusion (Puissant et *al.*, 2014). It was also necessary to select these samples separately to avoid overlap between the two sets in the same areas (Figure 3). In the remote sensing literature and statistics, a certain number of representative samples of the objects to be classified is needed to avoid over- or under-learning certain objects. For all classifications, 80% of the samples were used to train and tune the ML algorithms, while 20% of the validation samples were used as a test set.

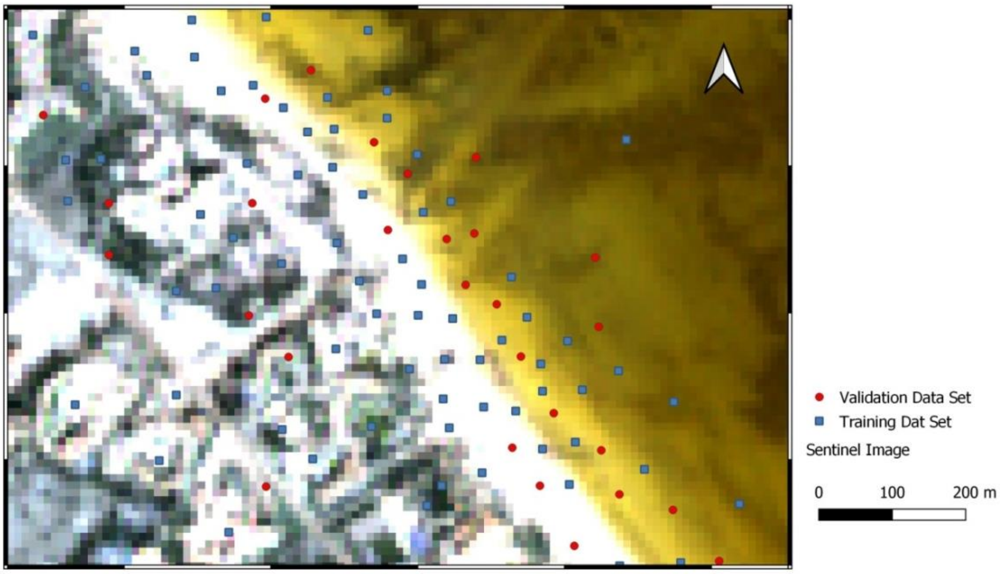

Fig. 3. Illustration of the distribution of validation and training samples on a Sentinel-2 image

3.3.2. Object-Based Image Analysis (OBIA)

OBIA is based on image objects consisting of pixels with homogeneous information (Hossain and Chen, 2019). This method provides spatial information as well as spectral, textural and contextual features as a basis for classification. It subdivides the image into homogeneous regions called image objects or segments (Benz et *al.,* 2004). The OBIA approach comprises three main stages: image segmentation, classification and validation.

3.3.2.1. Segmentation

Segmentation is the most crucial process in OBIA (Deliry et *al.*, 2021). Its principle is to automatically divide images into thousands of non-overlapping superpixels (Yang et *al.,* 2020). The result is well-defined regions or features of an object that can be distinguished. In the field of remote sensing, there are several segmentation algorithms. Our study compares two segmentation algorithms that were applied to segment coastal land cover types in order to extract water/land boundaries: mean shift segmentation (MSS) and multi-resolution segmentation (MRS).

Meanshift image segmentation (MSS)

The main idea behind this algorithm is to divide the image into highly correlated segments. The Orfeo Tool Box (OTB), an open-source software package, was used to apply MSS. Three parameters need to be determined: spatial radius (sr) used to determine the neighborhood boundaries, range radius (rr) for defining the width in spectral space, and minimum region size (mrs) to be maintained after clustering (Varo-Martínez and Navarro-Cerrillo, 2021). In our case, 13 trials were conducted. The parameters were set after cross-validation based on the segmentation models that achieved the highest overall accuracy (OA).

Multi-resolution image segmentation (MRS)

The MRS is one of the most widely used segmentation algorithms in the literature and was chosen for its proven accuracy in wetland classification (Hossain and Chen, 2019; Merchant, 2020; Yan et *al.,* 2021). The main objective of this algorithm is to reduce average pixel heterogeneity as much as possible (Incekara et *al.,* 2018). The MRS was implemented using the eCognition© Definiens Developer software. In order to obtain the expected results, three parameters had to be chosen empirically to demonstrate the morphology of the objects: scale parameter (Sc), representing the weighting between a colour factor (or spectral factor) and a shape factor, designated by the weight w shape/w colour; shape (Sp), defined as the maximum heterogeneity allowed within the objects; and compactness (Cp), making the object more or less regular, denoted by the weight w compt/w smooth.

Parameters were determined based on trial and error as well as the visual interpretation. In addition, the near-infrared (NIR) band of the Sentinel images and the mid-infrared (MIR) band of the Landsat image were more weighted (value of 10) than the other RGB bands (value of 1), as this region of the electromagnetic spectrum is known to enhance the detection of the land/water interface due to the inherent optical properties of water (Valderrama-Landeros and Flores-de-Santiago, 2019).

3.3.2.2. Classification

Classification is divided into two stages: training and prediction, and was done using eCognition software and an RF classifier (see *Random Forest Classifier* section)

3.3.3. Pixel-Based Image Analysis (PBIA)

The concept of the traditional PBIA method is based on the spectral information of satellite images. It involves assigning a thematic class to each pixel (Guo et *al.*, 2021) by assessing the degree of similarity of a pixel's spectrum to reference spectra for surface features (Shayeganpour et *al.*, 2021). PBIA was applied to detect the shoreline using the open-source software OTB.

The method consists of three steps. The first is classification using the RF algorithm, followed by validation and vectorization (see *Random Forest classifier* section). This approach produces raster maps with a 'salt and pepper' appearance (Mollick et *al.*, 2023). Using Mapla's Classification Map Regularization tool, smoothing was performed to transform 'isolated' pixels into the majority of surrounding pixels. The result of the classification was then converted from raster to vector format using the Polygonize Raster to Vector tool in QGIS. It consists of obtaining class boundaries to extract the shoreline. The extracted boundary was a raw vector layered with high-frequency noise.

Random Forest Classifier

The various approaches involved the evaluation of PBIA and OBIA based on an RF-supervised ML classifier. This type of model has several advantages, including the non-parametric nature of the algorithm, high classification accuracy and the ability to identify important variables and predict missing values (Jhonnerie et *al.*, 2015).

Given the performance and automatic aspect of the method, which requires only a few parameters to be set, quantifying the importance of the variables is one of the most crucial aspects of the model applied (Ramesh and Singh, 2020). Two parameters were examined: the maximum number of trees in the forest (Ntree) and the minimum number of samples in each node (Mtry). Published literature has highlighted that the RF classifier is more sensitive to the Mtry parameter than the Ntree parameter (Gonçalves et *al.,* 2020). The RF parameters were configured with Ntree and Mtry set values after cross-validation. We therefore tested different scenarios using the spectral bands (B1/B2/B3/B5) for the Landsat-5 TM image (1989) and (B2/B3/B4/B8) for the Sentinel-2 images (2015/2023). The iteration parameters that performed best in terms of OA were finally used to produce the final classification images. From the various Mtry values tested, the values of 30 and 50 were selected for PBIA-RF and OBIA-RF, respectively. Next, class prediction of the objects was performed using the *vector classifier* tool of the OTB software for the OBIA approach, and the *image classifier* tool for PBIA approche.

3.4.Shoreline detection and extraction using a deep learning model (CNN)

The convolutional neural network (CNN; Fukushima, 1988) is a highly responsive supervised DL algorithm. CNN is a powerful recognition algorithm widely used in pattern recognition and image processing that has the ability to learn autonomously and perform information extraction efficiently, quickly and reproducibly. However, the CNN-based method is more complex than other methods and requires purer images (Zhang et *al.,* 2016; Zhu et *al.*, 2017). Its architecture consists of convolutional, pooling and fully connected layers.

We used the new combination of CNN with the OBIA using the MRS approach developed by Bengoufa et *al.,* (2021b) for rocky shoreline extraction and Bengoufa et *al.*, (2023) for the extraction of shoreline biological indicators. We adapted this approach for the extraction of water/land boundaries. The aim is to implement a shoreline extraction method that integrates the benefits of CNN model output, namely CNN probability, with the robustness of the OBIA approach.

As well, for the classification process, our CNN architecture was fed with 2 × 2 sample patch sizes. Given this small size, the number of hidden layers was 1, with a convolution kernel size of 1 × 1. A max-pooling layer with a kernel size of 1× 1 was used after the first convolution layer. Max-pooling's role is to merge features that are semantically similar (Bengoufa et *al.*, 2021a). This is a non-linear top-down sampling technique that uses the maximum value of each cluster in the previous layer to reduce the loss of information in subsequent convolution layers.

In addition, the use of patch sizes of 50 and 5,000 training steps resulted in excellent performance. The learning rate parameter was set to 0.0006 after trial-and-error tests. Then different feature maps were generated.

The MRS was used for image segmentation. A class hierarchy was applied for all classes according to a linear cohesion function (x, y), with a maximum value equal to one (1) and a minimum equal to zero (0). The resulting objects from this segmentation were trained and classified based on a combination of neighbourhood, spatial features and similarity in the CNN probability (CNN application output), which can bring advantages in automatic data extraction and high-precision prediction. The resulting polygons (objects) were converted to polyline format to select and extract the target shoreline.

3.5.Detection and extraction of the shoreline using the band ratioing method

Boussetta et *al.*, (2022a) used the BR method to automatically extract the sandy shoreline of Jerba Island and obtained good results. To evaluate the accuracy of the machine and DL methods used here, we compare their results with those of the BR method.

For the BR method, the ratio between the visible NIR and MIR was calculated, corresponding to band 5/band 2 (MIR/green) in the case of Landsat TM (1989) and band 8/band 2 (NIR/green) in the case of Sentinel-2 images (2015–2023), as the NIR and MIR wavelengths are strongly absorbed by water and reflected by soil (Alesheikh et *al.*, 2007; Cui and Li, 2011). This initial BR processing was followed by three steps: reclassification and vectorization using tools from the IDRISI Selva system and smoothing, performed using ArcGIS software (Boussetta et *al.*, 2022a).

3.6.Sensitivity and accuracy assessment

3.6.1. Qualitative assessment

The qualitative evaluation of our methods was based on the visual adoption of classification maps. This assessment allowed us to gain an in-depth understanding of the process. It includes both the why and the how and allows us to delve deeper into topics of interest and explore subtleties.

3.6.2. Quantitative assessment

3.6.2.1. Confusion matrices and metrics

A confusion matrix was calculated to assess classification quality and detect confusion between well- and poorly-classified pixels. The main indices calculated from the generated matrix are the kappa index developed by Cohen (Cohen, 1960), which provides global measures of quality, and the OA index, which reflects classification performance. A visual assessment of the classification was combined with this numerical calculation to identify the sources of error. The accuracy percentage ranges from 0 to 1, with values close to 1 corresponding to very good OA. An index greater than 0.6 is considered good and an index greater than 0.8 is considered very well.

3.6.2.2. Comparison between extracted and reference shorelines

A reference shoreline was used to accurately assess the different methods used here. All detected shorelines were imported into ArcMap 10.4. The results of the (semi-)automatic extraction were then compared with the results of the manual digitization of the shoreline used as the reference. Manual digitization of the shoreline leverages the judgement and interpretation of scientists to identify the land-sea boundary, compared to computer-based classification methods (Matin and Hasan, 2021; Sreekesh et *al.*, 2020).

The digitization of the shorelines was performed manually from the Sentinel-2 and Landsat-5 images, as the separation of land surfaces and water bodies could be easily detected when visually inspecting the images. After digitizing the shorelines for the years 1989, 2015 and 2023, respectively, these digitized shorelines are used as a reference for calculating the net shoreline movement (NSM; equation 3) relative to the shoreline extracted from (semi-) automatic classification techniques. The shoreline change rates along the coastal zone were then calculated using the DSAS version 5.0 extension developed by the USGS.

$$NSM = timeoldest - timerecent \text{ (Eq. 3)}$$

In addition, the shoreline change rate expressed by the end point rate (EPR) was calculated using the extracted shorelines from each method and compared with the EPR obtained using the digitized shorelines (reference shorelines). This could include assessing the chosen method’s impact on the final erosion risk assessment.

3.7.Estimation of erosion rate (shoreline change rate)

The extracted shorelines are stored in a personal geodatabase in vector form. First, the buffer method was used to establish a baseline roughly parallel to the shoreline at an offshore distance of 200 m from the source. This shoreline was then used to draw 689 perpendicular transects with a spacing of 30 m. The distance between two shorelines on a transect represents the change in the shoreline between their corresponding points of intersection.

In order to determine long-term shoreline change statistics over a 34-year period (1989–2023), the EPR method was used with the Digital Shoreline Analysis System (DSAS) in ArcGIS10.4.1 software. The EPR method (equation 1) is calculated by dividing the distance of shoreline movement by the time elapsed between the oldest and the most recent shoreline (Himmelstoss et *al.,* 2018).

$$EPR = NSM/T \text{(Eq. 1)}$$

The erosion rate cannot be estimated without taking into account the total sources of error ($\boldsymbol{E\alpha}$), namely the error associated with remote sensing data processing (RMSe), the error of the automatic shoreline extraction from Landsat and Sentinel data based on the method used (MEe) and the uncertainty of the EPR calculations (EPRunc), according to the following equation 2:

$$\boldsymbol{E\alpha} = \sqrt{}RMSe^2 + MEe^2 + EPRunc^2 \qquad \text{(Eq.2)}$$

4. Results

Multisensor analyses using high spatial resolution optical images were used to compare different methods (BR, ML and DL techniques) for (semi-)automatic shoreline extraction and erosion risk assessment. The results were evaluated in terms of operator experience (qualitative and visual assessment) and performance and suitability through statistical analysis (quantitative assessment).

4.1.Shoreline detection using machine learning algorithms

Here, we present the results of the accuracy evaluation of all the methods used (PBIA-RF, OBIA-RF, CNN-OBIA and BR), together with the classification outputs for each method. The parameter fitting was done empirically.

4.1.1. Random Forest classification using PBIA (PBIA-RF)

Five classes were differentiated using the PBIA-RF approach for the Sentinel-2 composite images: water (1), land (2), urban (3) and vegetation (4; Figure 4), and four classes were identified on the Landsat-5 image (Figure 5): water (1), land (2), vegetation (3) and other (4).

The classification accuracy was evaluated using the confusion matrix to assess the quality of the predictions (Šiljeg et *al.*, 2022). The calculated confusion matrix includes commission errors, i.e., pixels included in other thematic classes after classification, and omission errors, i.e., thematic pixels lost after classification. The kappa index was equal to 0.87, meaning 87% of the ground-truth variables were correctly classified. The ground-truth classes correspond to the classes defined in the matrix column, and the classes of the classification result correspond to the rows of the matrix.

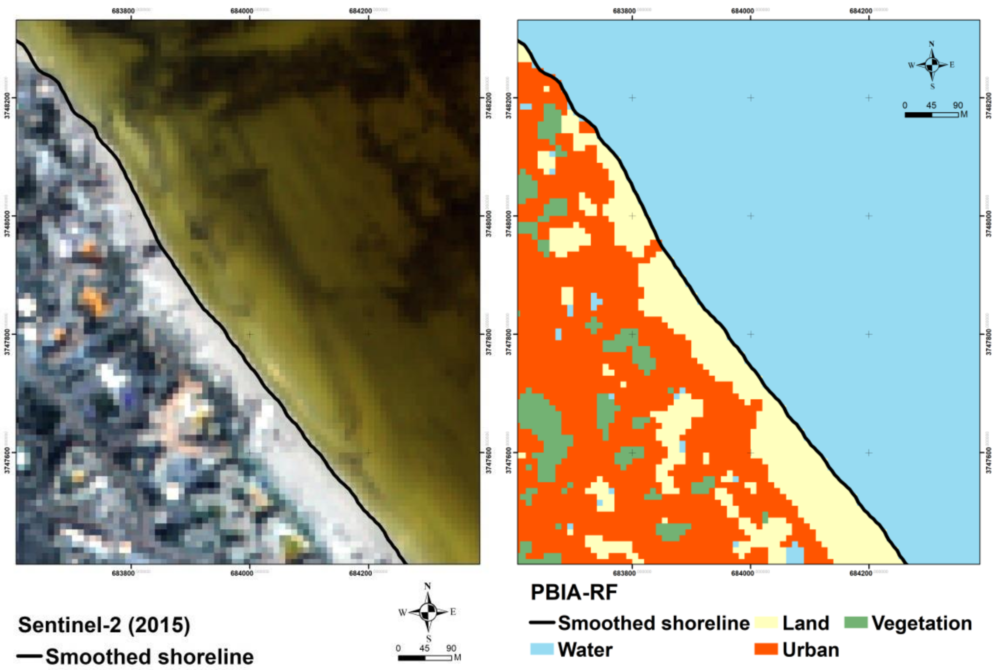

Fig. 4. PBIA classification maps using the RF algorithm Sentinel-2 image 08/12/2015

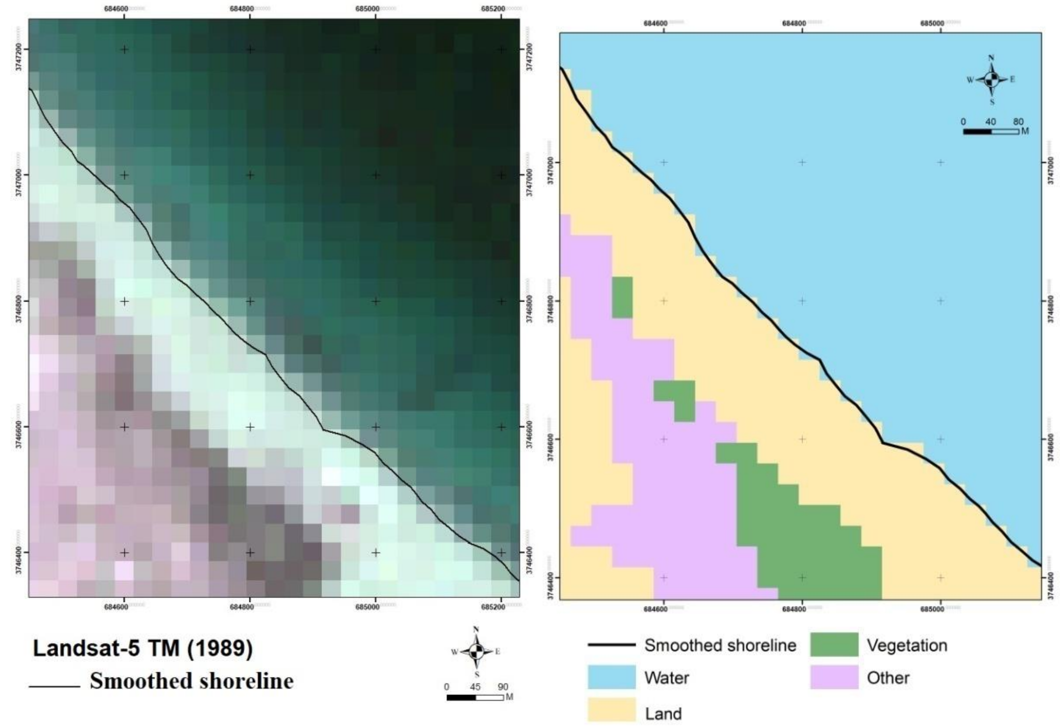

Fig. 5. PBIA classification maps using the RF algorithm Landsat-5 image 08/21/1989

4.1.2. Object Based Image Analysis using RF and CNN

4.1.2.1. *MSS segmentation*

Several segmentation tests were carried out, and the different parameters generated entirely different results. Based on visual inspection and the most suitable OA, the parameters of the MSS segmentation algorithms applied to Sentinel and Landsat images were optimized and set. Table 6 provides an overview of the results of the various parameter values and tests performed on Sentinel 2023 images.

The variation of the segmentation parameters of the MSS algorithm is directly correlated with the type of object detected by visual observation. The smaller the value of the sr and mrs parameters, the greater the number of segments (objects) generated. On the other hand, the larger the value of the parameter rr, the greater the loss of information, resulting in blurred objects of interest. This situation was confusing due to the large amount of data. Therefore, the parameter values sr, rr and mrs of 10, 0.05 and 20, respectively, were determined to be the best configuration parameters for the Sentinel-2 image (Table 6). These parameters of the MSS algorithm gave the best OA of 95%. For the Landsat-5 image, the parameters 10, 0.01 and 5 showed the best OA of 92.7%.

Table 2. Different MSS segmentation parameter values and test results for Sentinel-2023 images

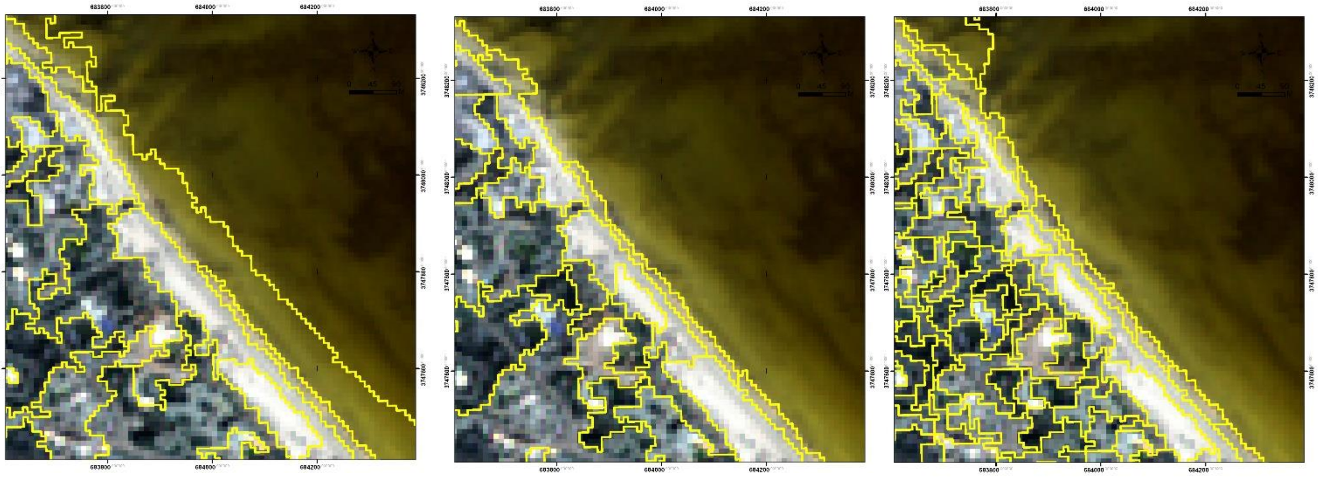

Parameters	Sr=30,rr=0.07, mrs=20	Sr=10, rr=0.1, mrs=50	Sr=10, rr=0.05, mrs=20
RF-OA (%)	75	82	95

4.1.2.2. MRS segmentation

The configuration tests (Table 7) applied to the multi-resolution segmentation (MRS) algorithm showed that the larger Sc, the larger the objects; the smaller Sp, the more objects are generated; and the larger Cp, the more objects are generated.

Therefore, values of 20, 0.1 and 0.5 were selected for Sc, Sp and Cp, respectively, for the Sentinel images. These configuration parameters were the best in terms of accuracy, achieving an OA of 96.3%. For the Landsat image, values of 0.9, 0 and 1 were selected for Sc, Sp and Cp, respectively, resulting in an OA of 94.6%.

Table 3. Results of MRS parameter setting on Landsat-5 images

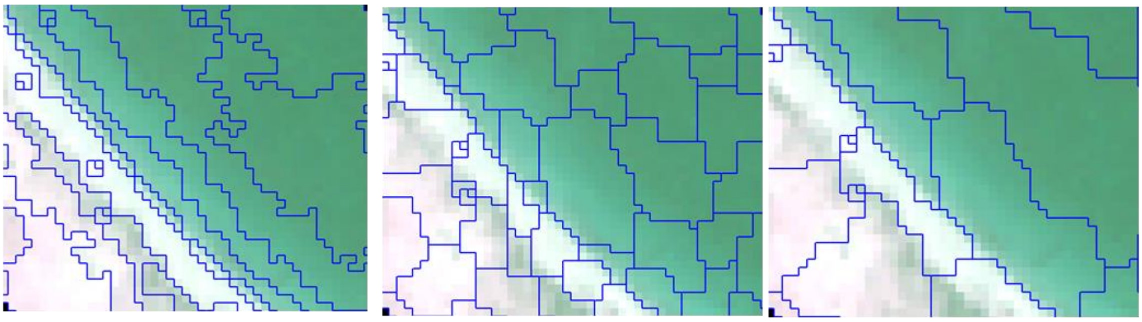

Parameters	Sc=0.9, Sp=0, Cp=1	Sc=0.9, Sp=0.1, Cp=0.1	Sc=2, Sp=0.1, Cp=0.1
RF-OA (%)	94.6	87.3	79.2

4.1.2.3. *Classification*

Similar to PBIA, four classes were identified for the Sentinel-2 images: water (1), land (2), urban (3) and vegetation (4; Figure 6), and for Landsat-5 images, four classes were identified: water (1), land (2), vegetation (3) and other (4; Figure 8). The use of different ML and DL algorithms (RF and CNN) with different types of segmentation (MSS and MRS) made it possible to determine the most suitable method for the satellite images used. Pronounced differences between the different classes could be observed on the classification maps.

Zone (X) of the Sentinel-2 (2023) image is used as a test zone to estimate the limitations and accuracy of the method (Figure 9). The RF algorithm represented this area (X) as an urban area, while it was considered dry sand by the CNN algorithm. Verification in the field and against a very high spatial resolution satellite image led to the visual observation that it was a building well described by the RF algorithm. The maps clearly showed several errors, including the misclassification of vegetation cover and urbanization. The CNN algorithm represented a large amount of vegetation cover (class 3) interspersed with small areas of water (class 1). The RF algorithm represented it as mainly dominated by an urban area (class 3) interspersed with vegetation cover, even for the land class (class 2), which was represented inconsistently and heterogeneously by the CNN, while it was represented evenly and homogeneously by the RF.

The same findings were shown in the Landsat image (Figure 8), where several errors were seen. In particular, the incorrect classification of land (class 2) into other classes (class 4) and the amount of vegetation (class 3) were almost absent from CNN.

As a result, the RF-OBIA-MSS algorithm better reflects the reality on the ground. It seems to have fewer ambiguities in the classifications and fewer errors for the wet sand class, which is a fundamental class and thus considered an indicator of shoreline detection for sandy beaches.

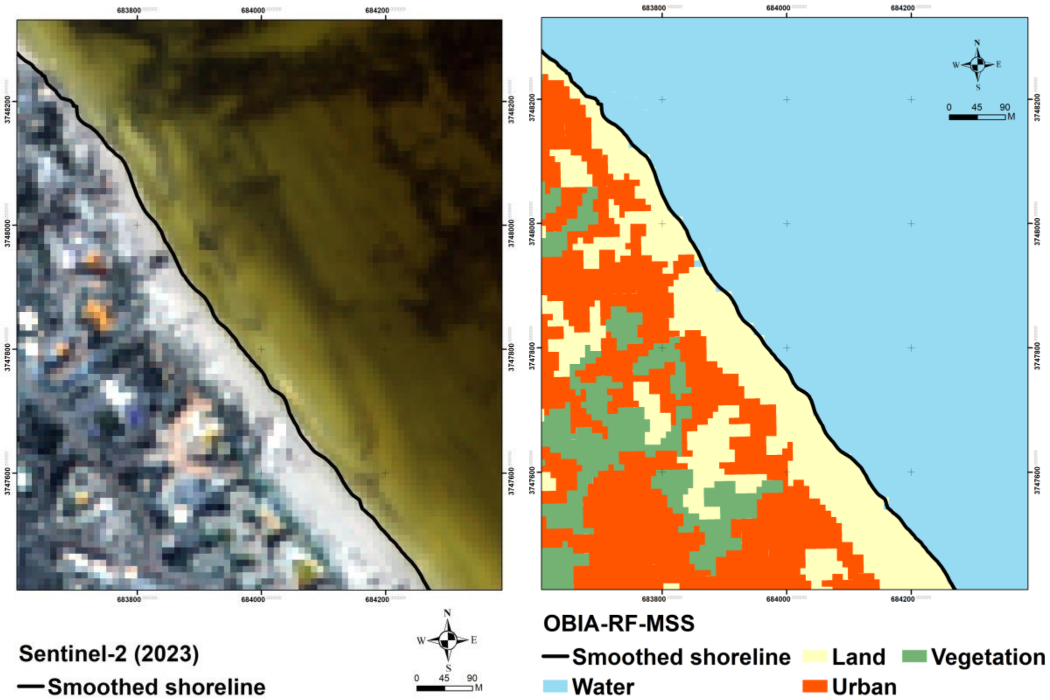

Fig. 6. OBIA-RF-MSS classification maps applied to Sentinel-2 (2023)

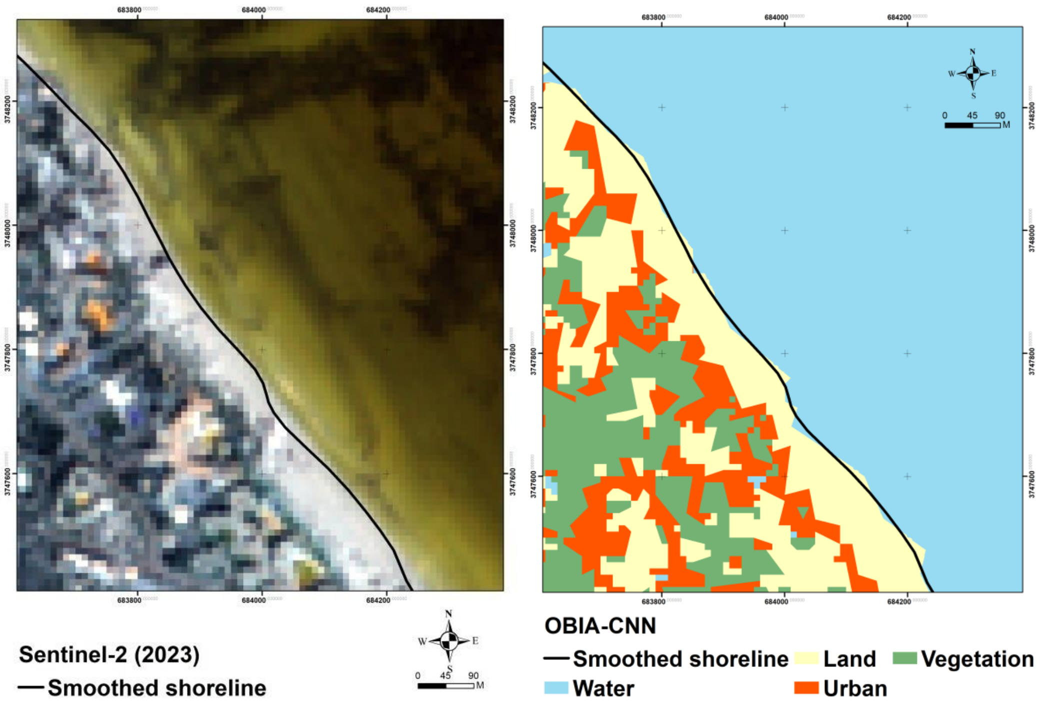

Fig. 7. CNN-OBIA classification maps applied to Sentinel-2 (2023)

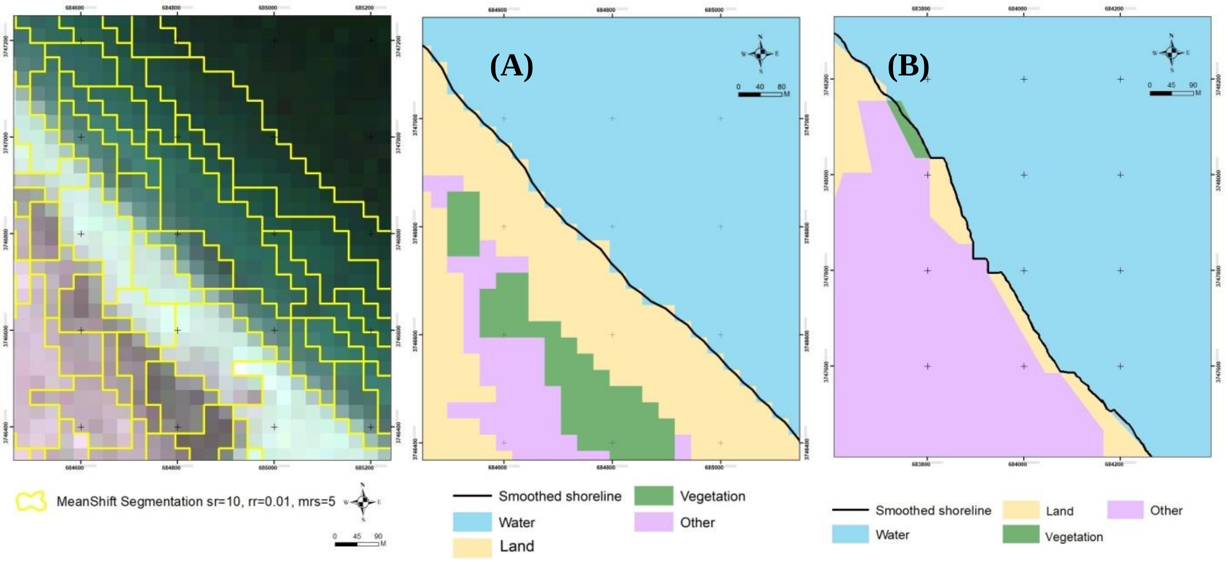

Fig. 8. Comparison of OBIA classification results applied to Landsat 1989 images using RF (A) and CNN (B) algorithms.

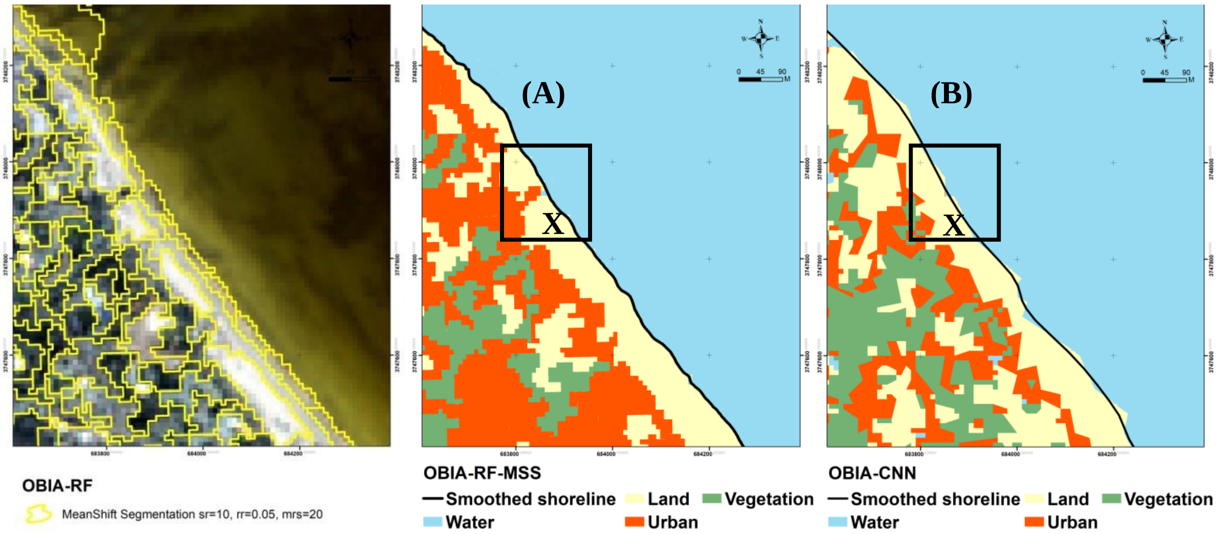

Fig. 9. Comparison of OBIA classification results applied to the Sentinel-2023 image using the RF (A) and CNN (B) algorithms.

4.1.3. Qualitative assessment

The classifications showed a satisfactory visual representation of the land cover. However, when comparing the RF-ML algorithm, the PBIA and OBIA approaches resulted in slightly different profiles. There were clear differences between the approaches to the representation of the vegetation class and the urban class. Despite these slight differences in representation between the different image analysis approaches, the water class was well defined overall.

The land class was also well represented. In contrast, differences in the representation of the vegetation class between the approaches were particularly striking. While the PBIA-RF approach accurately represented the land class, the OBIA-RF approach produced the most accurate representation of this same class along the shoreline. Since the boundary between land and water is the reference shoreline for shoreline detection, the OBIA-RF approach based on the MSS algorithm provided the best results.

4.1.4. Quantitative assessment

4.1.4.1. Accuracy of the classification model

The integrated approach based on a CNN and OBIA-DL model revealed the lowest kappa and global accuracy indices, with values below 0.8 and the lowest OA of 67%. This result is due to the high level of confusion between the different classes detected.

Since the kappa coefficient was above 0.8 for the classification approaches used (PBIA-RF and OBIA-RF; Table 8), the confusion matrix values have a high probability of validity. The PBIA and OBIA approaches both performed satisfactorily, with an OA above 85%. More specifically, OBIA-RF-MSS had the highest kappa index values of the other classification methods monitored. OBIA-RF achieved the highest OA of around 95%.

Table 8. Accuracy of different classification methods, kappa index and overall accuracy

	PBIA-RF			**OBIA-RF-MSS**			**OBIA-RF-MRS**			**CNN-OBIA**		
Image	1989	2015	2023	1989	2015	2023	1989	2015	2023	1989	2015	2023
Indice kappa	0.88	0.87	0.90	0.93	0.92	0.93	0.71	0.63	0.74	0.67	0.76	0.79
OA %	90%	89%	92%	92.7%	95%	95%	71%	69%	70%	67%	77%	78%

4.1.4.2. Accuracy of shoreline extraction

The comparison between the extracted shoreline and a digitized shoreline (reference) is presented in Table 9, which shows the NSM, which are the minimum, maximum and average (mean) distance calculations, namely the i) min, ii) max and iii) mean values. The mean distance is used as an ‘indicator ‘of the accuracy of the shoreline extraction method.

Using the PBIA approach, the RF algorithm resulted in a shoreline extraction with an average distance of 15.25 m for the Landsat image and 10 m for the Sentinel images.

Overall, the OBIA-RF-MSS approach generated shorelines with greater accuracy. It provided the most accurate shoreline extraction with mean distances of 7.8 m, 5.5 m and 6.09

m for Landsat-5 and Sentinel-2 images (2015, 2023), respectively. The BR approach produced shorelines with mean distances of 11.28 m, 7.7 m and 7.6 m for Landsat-5 (1989) and Sentinel-2 (2015, 2023) images, respectively.

The most significant distance values are observed with the combined CNN-OBIA approach, which has lower accuracy with mean distance values of 18.48 m, 8.14 m and 16 m for satellite images from 1989, 2015and 2023, respectively. These distances prove that this (semi-)automatic extraction method is completely ineffective in detecting the land/water boundary on Sentinel-2 and Landsat-5 TM images.

The final results of the methods used show that the OBIA-RF-MSS approach is the best for shoreline extraction. However, it should be noted that this small-scale detection is due to the high resolution of the Landsat and Sentinel images.

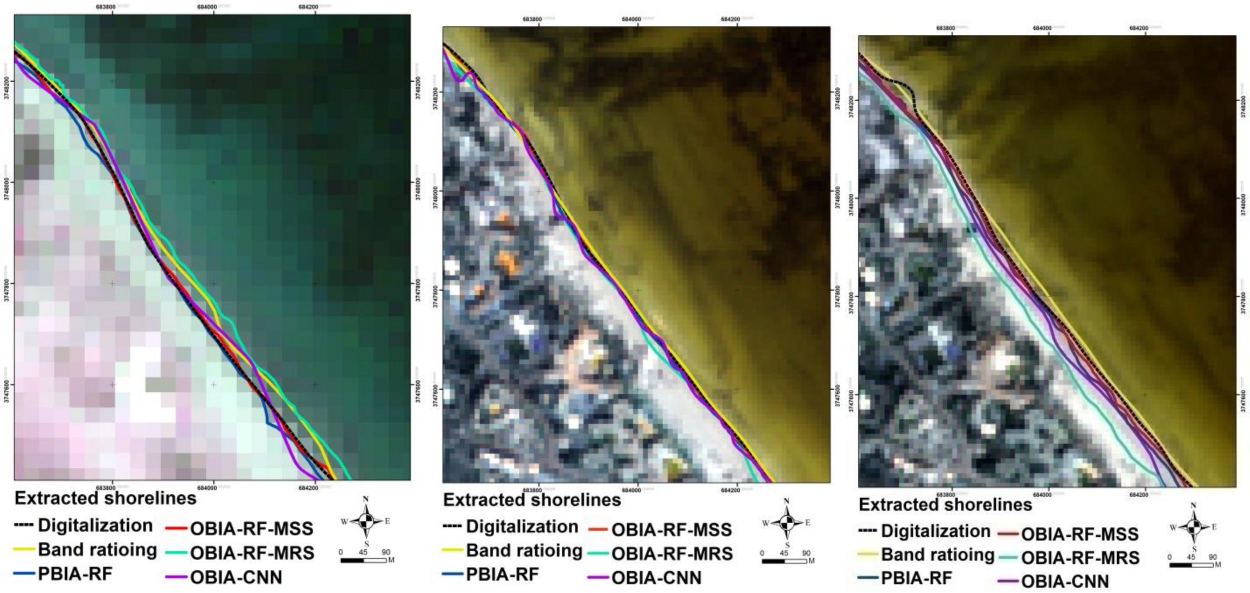

Fig. 10. Extracted shorelines from different methods (a) Landsat TM image 1989 (b) Sentinel-2 image 2015 (c) Sentinel-2 image 2023

Table 9. Net shoreline movement (NSM) statistics based on DSAS calculations relative to the reference shoreline

	Landsat-5 1989					**Sentinel-2 2015**					**Sentinel-2 2023**				
NSM	Ratio	PBIA-RF	OBIA-RF-MSS*	OBIA-RF-MRS	CNN-OBIA	Ratio	PBIA-RF	OBIA-RF-MSS	OBIA-RF-MRS**	CNN-OBIA	Ratio	PBIA-RF	OBIA-RF-MSS	OBIA-RF-MRS	CNN-OBIA
MIN	0.1	0.8	0.01	0.8	0.01	0.01	0.02	0.03	0.03	0.02	0.02	0.02	0.03	0.05	0.11
MAX	59	50.02	53	54	99.78	40	37.42	35.33	40	45	39	38.2	38.11	40	52
MEAN	**11.28**	**15.25**	**7.8**	**10.11**	**18.48**	**7.7**	**10**	**5.5**	**8.5**	**8.14**	**7.6**	**10**	**6.09**	**8.01**	**16**

**Mean Shift Segmentation **Multi-resolution Segmentation*

The various methods of BR, PBIA-RF, OBIA-RF-MSS, OBIA-RF-MRS, CNN-OBIA and digitization show the EPR, or the average rates of shoreline change, for the east coast of Jerba between 1989 and 2023 (Table 10). The graph (Figure 11) presents an overview of the different evolution rate values (EPR) results for each method used. Form Table 10 and Figure 11, we can note that OBIA-MSS with the RF algorithm obtained values closest to those of the EPR of the digitization method, which is our reference EPR used to evaluate the results. Therefore, OBIA-RF-MSS is more relevant than the other methods.

Table 10. Comparison of different End Point Rate of the shoreline extracted from the used methods

EPR (m/year)	**BR**	**PBIA-RF**	**OBIA-RF-MSS***	**OBIA-RF-MRS**	**CNN-OBIA**	**DIGITIZATION**
MIN	-4.9	-4.62	-4.1	-4.82	-4.8	-4.06
MAX	+41.5	+43.2	+39.97	+43.5	+42.32	+39.32
MEAN	-1.38	-1.36	-0.8	-1.39	-1.8	-0.77

**Mean Shift Segmentation*

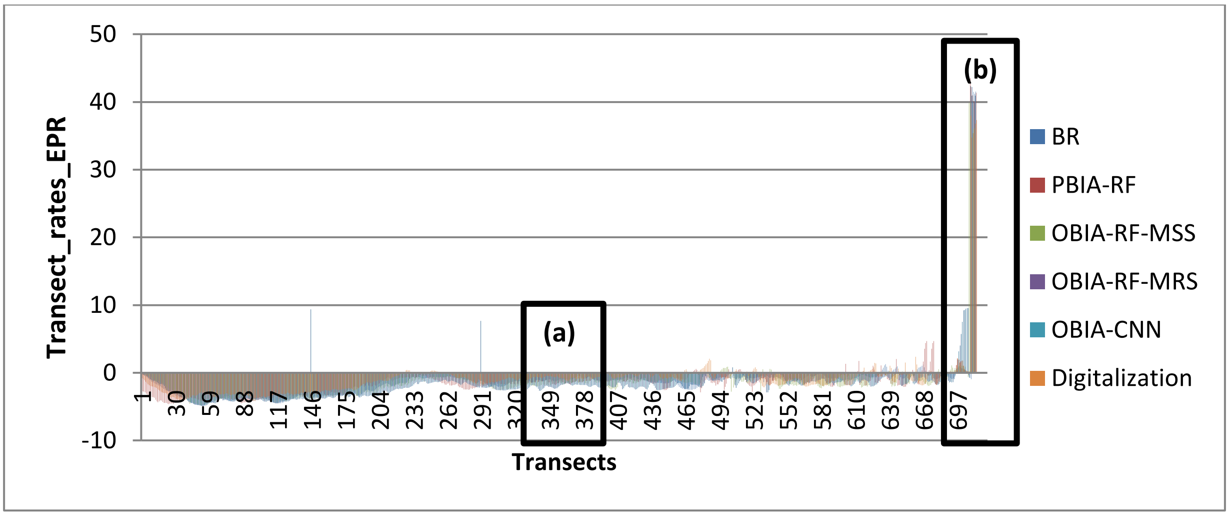

Fig. 11. The rate of change of sandy beaches (a) and sandy spit (b) on the east coast of Jerba Island between 1989 and 2023

4.2.Shoreline change rate: Erosion risk assessment

Analysis of shoreline evolution over the 727 transects and after applying an overall margin of error for the methods adopted of about ±2.38m for sandy beaches and ±3.16 m for the sandy spit revealed a clear trend of erosion throughout the entire study area, with the exception of the Rass Rmel sand spit, which experienced a sharp increase with a maximum evolution of about +39.97 m/year. The results of this study are shown in Figure 12. Positive (+) and negative (-)

EPR values indicate accretion and erosion, respectively, in a particular region on the island's east coast.

5. Discussion

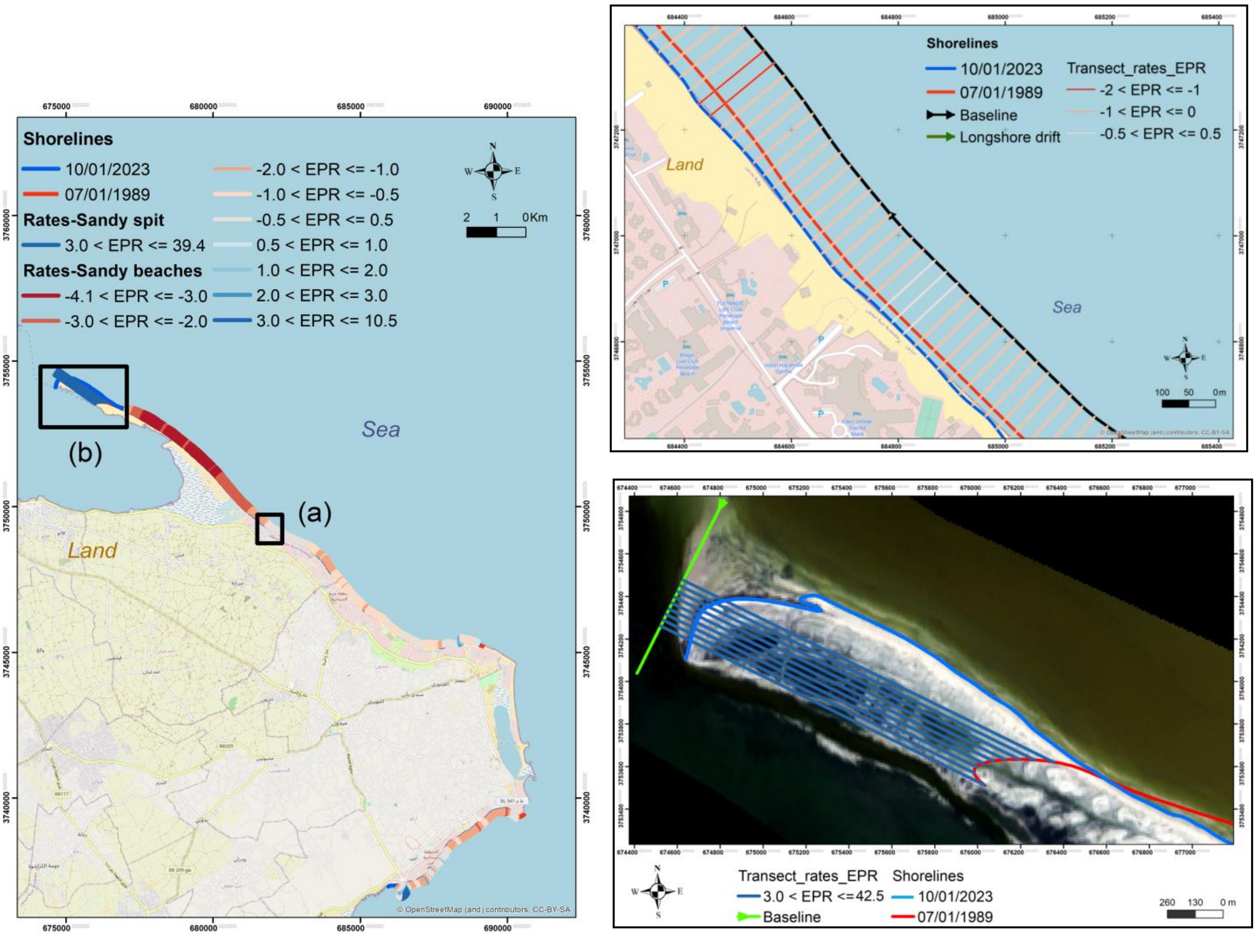

Fig. 12. The rate of change of shorelines extracted from OBIA-RF-MSS recorded with the EPR method in front of the Radisson Hotel on the east coast of Jerba (a) and for the sand spit at Rass Rmel (b)

Optical imagery has been found to be more feasible for capturing shoreline positions at different spatial and temporal scales (Almonacid-Caballer et *al.*, 2016; Hegde and Akshaya, 2015). The methodological approaches developed for shoreline extraction were based on high-resolution open-source optical imagery, namely Landsat-5 TM (30 m) and Sentinel-2 (10 m).The aim was to analyze and assess the land cover and to extract and distinguish the different classes.

Approaches based on band ratios are widely used in shoreline monitoring and extraction studies (Tsiakos and Chalkias, 2023b). In the previous technology, green and NIR bands were used to define threshold values separating water pixels from land pixels (Cham et *al.*, 2020). In the present work, the ratio method based on visible (band 2) and MIR-NIR (bands 5 and 8) shows good results for shoreline detection. These results are similar to those obtained by Roy et *al.*, (2018), which showed that the Band ratioing method yields significant results for the delineation of the shoreline over a 25-year period.

In contrast, this method allows deficient detection of sandy shorelines on satellite imagery. This simple and fast method does not require user intervention (Boussetta et *al.*, 2022a). However, this approach has certain limitations and can lead to questionable results when monitoring applications in a complex environment such as a sandy spit. BR is still a primary method. With this in mind, the main objective of this work was to develop and compare methods to define an effective and validated approach for more systematic and detailed monitoring of coastal dynamics, taking advantage of the latest innovations in remote sensing, DL and shallow ML.

5.1.Images analysis for shoreline extraction

A comparison of the three approaches to satellite image classification was carried out to determine the best one. We tested two classification methods, OBIA and PBIA, to detect coastal land cover types. The OBIA approach provided a more convergent representation of land cover. This finding is consistent with the results of studies by Mollick et *al.,* (2023), who argued that the accuracy of OBIA was 27% higher than that of PBIA. Furthermore, comparing the CNN-OBIA approach with the ML algorithm-based OBIA approach indicates that the OBIA-RF approach performs better than the CNN-OBIA approach and has higher accuracy. These results differ from those obtained by the studies of Zaabar et *al.,* (2022), who showed that CNN combined with object-based image analysis (OBIA), tested on Sentinel-2 spectral data, is the best-performing method for detecting different land-use classes with an OA higher than that of the OBIA-RF method by 0.9%.

If we compare the results of the method proposed in this article with those of Bengoufa et *al.,* (2021a), who demonstrated that the OBIA-RF method using the MRS algorithm, applied to very high-resolution images, performs best for shoreline extraction, this could be explained by the very high resolution of the Pleiade images (2m) and the medium resolution of the Landsat-5 TM and Sentinel-2 images (30 m and 10 m, respectively). Therefore, we can confirm that such a result depends on the data used, the classes targeted, the choice of the reference shoreline, and, above all, the user’s experience.

In OBIA, objects are extracted through segmentation processes that take into account the spectral, textural and contextual information of similar pixels (Blaschke, 2010). Moreover, despite the CNN algorithm’s ability to improve classification by selecting input features and OBIA, it is essential to consider the influence of different parameters on the segmentation processes. To be sure, the OBIA method should be enhanced by optimizing the segmentation parameters. Adjusting the parameters of the segmentation algorithms makes OBIA a subjective task (Belgiu et *al.,* 2014; Belgiu and Drăguţ, 2014), which was confirmed in this work after a good 10 adjustment attempts. However, cross-validation of Landsat and Sentinel-2 images removed this subjectivity. According to the results obtained, OBIA from MSS improved the classification and finally allowed a better shoreline extraction with a maximum OA value of 0.95 applied to the Sentinel-2 image.

It is important to note that the shorelines produced by all algorithms using the PBIA or OBIA approaches showed satisfactory results overall, with some interpretation errors in certain irregularly shaped coastal areas, especially for OBIA combined with CNN with a minimum OA of 0.77. Contrary to the studies carried out by Bengoufa et *al.,* (2021b) which showed that the combination of the deep learning model and OBIA are very effective for the extraction of the rocky shoreline using very high-resolution multispectral images. Also the results obtained with the CNN algorithm contradict the conclusions of the work of Gomez-de la Pena et *al.,* (2023), which presented an in-depth research and description of deep learning model configurations that proved effective for shoreline prediction.

5.2. A method for automatic shoreline extraction: user-friendliness and accuracy

The assessment of the performance of the methods applied to Landsat-5 and Sentinel-2 imagery reveals that shallow learning algorithms outperform DL techniques. OBIA-RF still has the highest percentages for parameter sensitivity, execution time, processing time and accuracy. In contrast, the BR method had the lowest percentages and a reasonable value for accuracy (28%), compared to the other approaches. The latter gives good results and, above all, saves a great deal of time. However, OBIA-RF brings added value in metric accuracy and extraction capacity. These results are similar to those obtained by Sreekesh et *al.,* (2020) who claimed that this method proved robust, with 95-99% consistency in areas presenting complex coastal geomorphological features (in our case the sandy spit), as well as when using satellite images of variable spatial resolution (medium- and high-resolution).

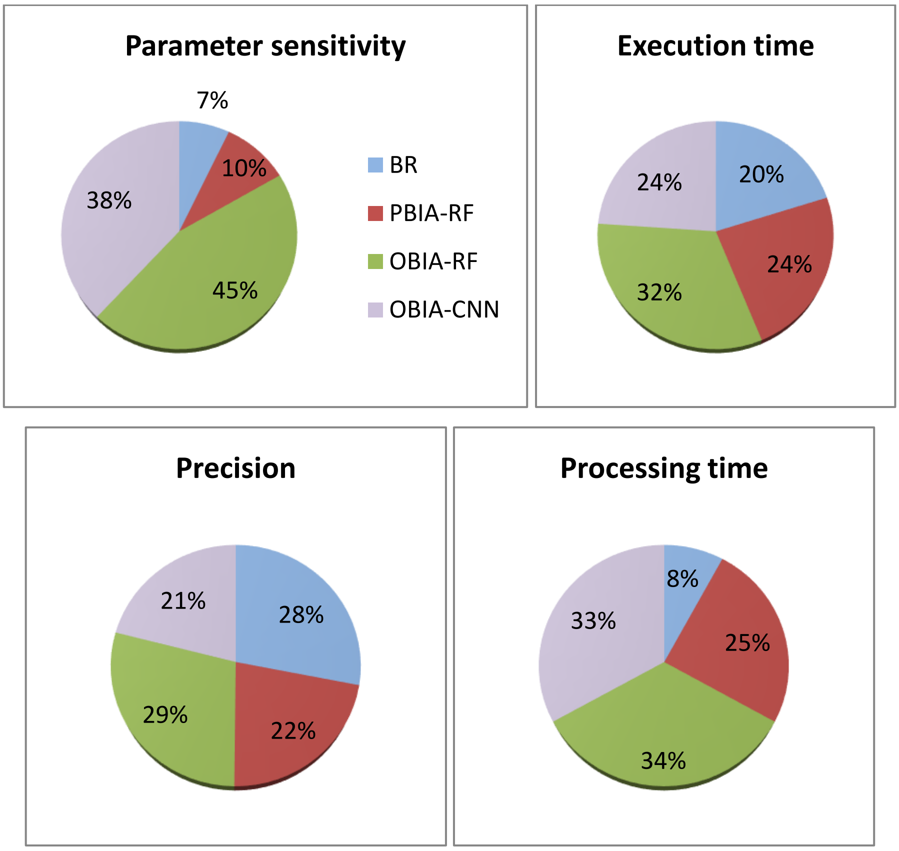

Fig. 13. Qualitative assessment of the performance of shoreline extraction methods

The shoreline extraction methods were continued by calculating the distances between the shorelines. The average value was used as a baseline for comparison. This evaluation also quantitatively shows the quality of each classification compared to another based on shorelines extracted along the line of each land use feature. In Figures 14 (a) and 14 (b) below, a small distance from the mean corresponds to a good classification, and vice versa. There is a clear difference between OBIA and PBIA and between the ML (RF) and DL (CNN) algorithms for land-water boundary classification. This difference proves that the OBIA-RF approach classifies our thematic variables better than the other approaches, especially at the wet sand class level.

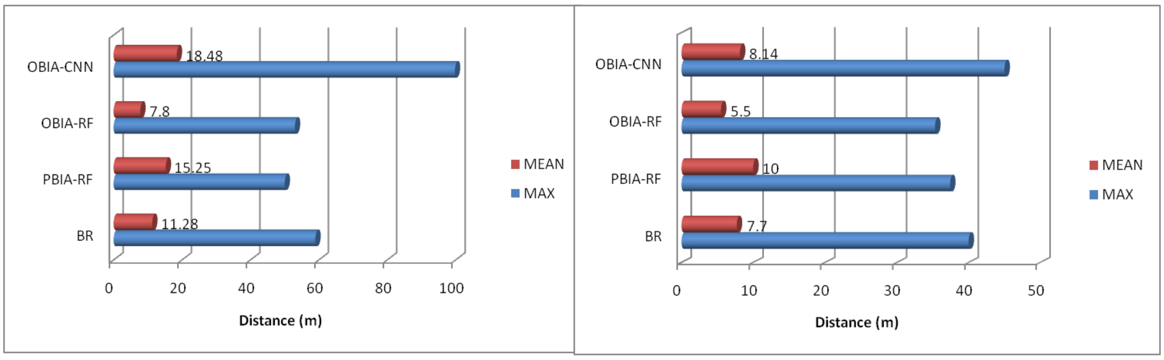

Fig. 14. Average and maximum distance between the extracted shoreline and the one digitized on the Landsat-1989 (a) and Sentinel 2015 (b) images

The sandy beaches have been subject to severe shoreline recession over the last three decades (1989–2023), except for the Rass Rmel spit, which has experienced significant sediment accretion (+39.97 m/year between 1989–2023). This apparent trend towards erosion and accretion was well illustrated by the work of Boussetta et *al.,* (2022a), where the DSAS results are conform to the real-world situation. The results of the retrospective analysis of the shoreline change, leads us to raise the alarm about the situation of the sandy beaches on the island of Jerba, given the exacerbation of the phenomenon of erosion. This phenomenon is changing the hydrological and the sediment transport balances which is causing landslides. This can have serious consequences for biodiversity, socio-economical security and for the humane safety living in the immediate vicinity of these environments. This situation is more complex for our study area, given that the island of Jerba is very frequented as it is an excellent tourist destination, where most of the socio-economic activities are located close to the shoreline. This requires immediate awareness by managers and the involved stakeholders, in order to draw up natural risk prevention plans, especially in the context of the acceleration of sea level rise due to climate warming and global environmental change. The latter are increasingly felt in island environments such as our study area, which makes it as naturally very vulnerable (Boussetta et *al.,* 2022b).

Although the latter method has yielded good results, no study has provided statistics on the evolution rates of the different approaches. Therefore, this study is the first to provide, compare and, most importantly, validate the EPR, or the shoreline evolution rates, for the Jerba Island over a 34-year period. The outputs of this study could be a good tools for coastal management and risk mitigation.

6. Conclusions

The analysis of satellite images to determine an appropriate land cover detection method is vital for extracting relevant information to monitor the evolution of the shoreline. Before choosing the method of detecting and extracting the reference shoreline, it is important to eliminate distortions due to the irregular shape of the land. Therefore, the radiometric and geometric corrections were carried out thoroughly. In order to select the detection methods for the different classes according to research needs, field visits and visual interpretations were considered preparatory steps in this work. They allowed us to identify the objects and structures in the field on the east coast of Jerba.

The comparison of the different classification techniques (BR, PBIA-RF, OBIA-RF and CNN-OBIA) enabled us to understand their effectiveness and efficiency by comparing their OA and kappa index statistics. The qualitative and quantitative evaluation and the validation process using the digitization method produced the best results. The OBIA-RF-MSS classification proved the most suitable, and the evaluation revealed that the real situation on the field is clearly the same.

Whether the method is basic or evolved, developing new methodologies in line with the available data and research objectives is critical. With this in mind, this study focused on establishing an operational, perfectly reproducible and less subjective shoreline detection method.

Using multitemporal, multisensory satellite imagery, we were able to determine a shoreline of 22.8 km, or over 15% of the island’s shoreline, with very high accuracy using the methodology created in this study. Statistical analysis of the EPR method using the DSAS tool allowed us to distinguish two types of situations. Some sites are experiencing general erosion (sandy beaches), and others are experiencing progradation (the Rass Rmel sand spit). These coastal forms are characterized by one or more eroding sectors: the upstream drifting part (the tourist area), feeding the downstream drifting part (the Rass Rmel spit) and a prograding part with occasional hook construction. In many places, erosion has become almost irreversible, and restoring stability will not be easy.

This work demonstrates the potential of Landsat-5 TM and Sentinel-2 imagery for obtaining shorelines from classifications on the sandy coasts of Jerba Island, where the indicator is the land-water boundary. This research is considered the first in its field to be applied to the Jerba study area, given its importance on a national scale. The final results should prove useful to coastal managers of island environments, which will increase awareness of the environmental problems on Jerba’s east coast and facilitate the implementation of plans to combat coastal erosion. Thanks to increased social awareness and data dissemination, this action will be much easier.

Credit authorship contribution statement

Amina BOUSSETTA: Conceptualization, Acquisition of data, Methodology, Software, Writing - Original Draft, Writing, Writing - Review & Editing. **Simona NICULESCU**: Resources, Visualization, Funding acquisition, Writing - Review & Editing. **Soumia BENGOUFA**: Validation, Writing - Original Draft, Writing - Review & Editing**. Mohamed Faouzi ZAGRARNI**: Supervision, Project administration, Writing - Review & Editing.

Acknowledgment

The authors are very grateful to the CNES/ TOSCA project ID 7618.

Funding

This work was supported by the University of Gabès as part of a work-study award.

References

Abdelhady, H.U., Troy, C.D., Habib, A., Manish, R., 2022. A Simple, Fully Automated Shoreline Detection Algorithm for High-Resolution Multi-Spectral Imagery. Remote Sens. 14, 557. https://doi.org/10.3390/rs14030557

Aedla, R., Dwarakish, G.S., Reddy, D.V., 2015. Automatic Shoreline Detection and Change Detection Analysis of Netravati-GurpurRivermouth Using Histogram Equalization and Adaptive Thresholding Techniques. Aquat. Procedia, INTERNATIONAL CONFERENCE ON WATER RESOURCES, COASTAL AND OCEAN ENGINEERING (ICWRCOE’15) 4, 563–570. https://doi.org/10.1016/j.aqpro.2015.02.073

Alesheikh, A.A., Ghorbanali, A., Nouri, N., 2007. Coastline change detection using remote sensing. Int. J. Environ. Sci. Technol. 4, 61–66. https://doi.org/10.1007/BF03325962

Almonacid-Caballer, J., Sánchez-García, E., Pardo-Pascual, J.E., Balaguer-Beser, A.A., Palomar-Vázquez, J., 2016. Evaluation of annual mean shoreline position deduced from Landsat imagery as a mid-term coastal evolution indicator. Mar. Geol. 372, 79–88. https://doi.org/10.1016/j.margeo.2015.12.015

Belgiu, M., Drăguţ, L., 2014. Comparing supervised and unsupervised multiresolution segmentation approaches for extracting buildings from very high resolution imagery. ISPRS J. Photogramm. Remote Sens. 96, 67–75. https://doi.org/10.1016/j.isprsjprs.2014.07.002

Belgiu, M., Drăguţ, L., Strobl, J., 2014. Quantitative evaluation of variations in rule-based classifications of land cover in urban neighbourhoods using WorldView-2 imagery. ISPRS J. Photogramm. Remote Sens. 87, 205–215. https://doi.org/10.1016/j.isprsjprs.2013.11.007

Bengoufa, S., Niculescu, S., Mihoubi, M.K., Belkessa, R., Abbad, K., 2023. Automatic Detection of Hydrodynamical and Biological Indicators of the Shoreline Using a Convolutional Neural Network, in: Niculescu, S. (Ed.), European Spatial Data for Coastal and Marine Remote Sensing. Springer International Publishing, Cham, pp. 191–205. https://doi.org/10.1007/978-3-031-16213-8_11

Bengoufa, S., Niculescu, S., Mihoubi, M.K., Belkessa, R., Abbad, K., 2021. ROCKY SHORELINE EXTRACTION USING A DEEP LEARNING MODEL AND OBJECT-BASED IMAGE ANALYSIS. Int. Arch. Photogramm. Remote Sens. Spat. Inf. Sci. XLIII-B3-2021, 23–29. https://doi.org/10.5194/isprs-archives-XLIII-B3-2021-23-2021

Bengoufa, Soumia, Niculescu, S., Mihoubi, M.K., Belkessa, R., Rami, A., Rabehi, W., Abbad, K., 2021. Machine learning and shoreline monitoring using optical satellite images: case study of the Mostaganem shoreline, Algeria. J. Appl. Remote Sens. 15. https://doi.org/10.1117/1.JRS.15.026509

Benz, U.C., Hofmann, P., Willhauck, G., Lingenfelder, I., Heynen, M., 2004. Multi-resolution, object-oriented fuzzy analysis of remote sensing data for GIS-ready information. ISPRS J. Photogramm. Remote Sens., Integration of Geodata and Imagery for Automated Refinement and Update of Spatial Databases 58, 239–258. https://doi.org/10.1016/j.isprsjprs.2003.10.002

Boak, E.H., Turner, I.L., 2005. Shoreline Definition and Detection: A Review. J. Coast. Res. 214, 688–703. https://doi.org/10.2112/03-0071.1

Boussetta, A., Niculescu, S., Bengoufa, S., Mejri, H., Zagrarni, M.F., 2022b. Assessment of Coastal Vulnerability to Erosion Risk Using Geospatial and Remote Sensing Methods (Case of Jerba Island, Tunisia), in: Niculescu, S. (Ed.), European Spatial Data for Coastal and Marine Remote Sensing. Springer International Publishing, Cham, pp. 113–132. https://doi.org/10.1007/978-3-031-16213-8_7

Boussetta, A., Niculescu, S., Bengoufa, S., Zagrarni, M.F., 09/2022a. Spatio-temporal analysis of shoreline changes and erosion risk assessment along Jerba island (Tunisia) based on remote-sensing data and geospatial tools. Reg. Stud. Mar. Sci. 55, 102564. https://doi.org/10.1016/j.rsma.2022.102564

Cham, D.D., Son, N.T., Minh, N.Q., Thanh, N.T., Dung, T.T., 2020. An Analysis of Shoreline Changes Using Combined Multitemporal Remote Sensing and Digital Evaluation Model. Civ. Eng. J. 6, 1–10. https://doi.org/10.28991/cej-2020-03091448

Cohen, J., 1960. A Coefficient of Agreement for Nominal Scales. Educ. Psychol. Meas. 20, 37–46. https://doi.org/10.1177/001316446002000104

Cui, B.-L., Li, X.-Y., 2011. Coastline change of the Yellow River estuary and its response to the sediment and runoff (1976–2005). Geomorphology 127, 32–40. https://doi.org/10.1016/j.geomorph.2010.12.001

Dang, K.B., Dang, V.B., Ngo, V.L., Vu, K.C., Nguyen, H., Nguyen, D.A., Nguyen, T.D.L., Pham, T.P.N., Giang, T.L., Nguyen, H.D., Hieu Do, T., 2022. Application of deep learning models to detect coastlines and shorelines. J. Environ. Manage. 320, 115732. https://doi.org/10.1016/j.jenvman.2022.115732

Deliry, S.I., Avdan, Z.Y., Avdan, U., 2021. Extracting urban impervious surfaces from Sentinel-2 and Landsat-8 satellite data for urban planning and environmental management. Environ. Sci. Pollut. Res. 28, 6572–6586. https://doi.org/10.1007/s11356-020-11007-4

Demir, N., Oy, S., Erdem, F., Şeker, D.Z., Bayram, B., 2017. INTEGRATED SHORELINE EXTRACTION APPROACH WITH USE OF RASAT MS AND SENTINEL-1A SAR IMAGES. ISPRS Ann. Photogramm. Remote Sens. Spat. Inf. Sci. IV-2/W4, 445–449. https://doi.org/10.5194/isprs-annals-IV-2-W4-445-2017

Erdem, F., Bayram, B., Bakirman, T., Bayrak, O.C., Akpinar, B., 2021. An ensemble deep learning based shoreline segmentation approach (WaterNet) from Landsat 8 OLI images. Adv. Space Res. 67, 964–974. https://doi.org/10.1016/j.asr.2020.10.043

Fukushima, K., 1988. Neocognitron: A hierarchical neural network capable of visual pattern recognition. Neural Netw. 1, 119–130. https://doi.org/10.1016/0893-6080(88)90014-7

Gomez-de la Pena, E., Coco, G., Whittaker, C., Montano, J., 2023. On the use of Convolutional Deep Learning to predict shoreline change. EGUsphere 1–24. https://doi.org/10.5194/egusphere-2023-958

Gonçalves, G., Andriolo, U., Gonçalves, L., Sobral, P., Bessa, F., 2020. Quantifying Marine Macro Litter Abundance on a Sandy Beach Using Unmanned Aerial Systems and Object-Oriented Machine Learning Methods. Remote Sens. 12, 2599. https://doi.org/10.3390/rs12162599

Görmüş, T., Ayat, B., Aydoğan, B., Tătui, F., 2021. Basin scale spatiotemporal analysis of shoreline change in the Black Sea. Estuar. Coast. Shelf Sci. 252, 107247. https://doi.org/10.1016/j.ecss.2021.107247

Guariglia, A., Buonamassa, A., Losurdo, A., Saladino, R., Trivigno, M.L., Zaccagnino, A., Colangelo, A., 2006. A multisource approach for coastline mapping and identification of shoreline changes 10.

Guo, S., Du, P., Xia, J., Tang, P., Wang, X., Meng, Y., Wang, H., 2021. Spatiotemporal changes of glacier and seasonal snow fluctuations over the Namcha Barwa–Gyala Peri massif using object-based classification from Landsat time series. ISPRS J. Photogramm. Remote Sens. 177, 21–37. https://doi.org/10.1016/j.isprsjprs.2021.04.018

Hegde, A.V., Akshaya, B.J., 2015. Shoreline Transformation Study of Karnataka Coast: Geospatial Approach. Aquat. Procedia, INTERNATIONAL CONFERENCE ON WATER RESOURCES, COASTAL AND OCEAN ENGINEERING (ICWRCOE'15) 4, 151–156. https://doi.org/10.1016/j.aqpro.2015.02.021

Himmelstoss, E.A., Henderson, R.E., Kratzmann, M.G., Farris, A.S., 2018. Digital Shoreline Analysis System (DSAS) version 5.0 user guide (USGS Numbered Series No. 2018–1179), Digital Shoreline Analysis System (DSAS) version 5.0 user guide, Open-File Report. U.S. Geological Survey, Reston, VA. https://doi.org/10.3133/ofr20181179

Hossain, M.D., Chen, D., 2019. Segmentation for Object-Based Image Analysis (OBIA): A review of algorithms and challenges from remote sensing perspective. ISPRS J. Photogramm. Remote Sens. 150, 115–134. https://doi.org/10.1016/j.isprsjprs.2019.02.009

Incekara, A.H., Seker, D.Z., Bayram, B., 2018. Qualifying the LIDAR-Derived Intensity Image as an Infrared Band in NDWI-Based Shoreline Extraction. IEEE J. Sel. Top. Appl. Earth Obs. Remote Sens. 11, 5053–5062. https://doi.org/10.1109/JSTARS.2018.2875792

Islam, Md.S., Uddin, Md.A., Hossain, M.A., 2021. Assessing the dynamics of land cover and shoreline changes of Nijhum Dwip (Island) of Bangladesh using remote sensing and GIS techniques. Reg. Stud. Mar. Sci. 41, 101578. https://doi.org/10.1016/j.rsma.2020.101578

Jhonnerie, R., Siregar, V.P., Nababan, B., Prasetyo, L.B., Wouthuyzen, S., 2015. Random Forest Classification for Mangrove Land Cover Mapping Using Landsat 5 TM and Alos Palsar Imageries. Procedia Environ. Sci. 24, 215–221. https://doi.org/10.1016/j.proenv.2015.03.028

Luijendijk, A., Hagenaars, G., Ranasinghe, R., Baart, F., Donchyts, G., Aarninkhof, S., 2018. The State of the World's Beaches. Sci. Rep. 8, 6641. https://doi.org/10.1038/s41598-018-24630-6

Matin, N., Hasan, G.M.J., 2021. A quantitative analysis of shoreline changes along the coast of Bangladesh using remote sensing and GIS techniques. CATENA 201, 105185. https://doi.org/10.1016/j.catena.2021.105185

McAllister, E., Payo, A., Novellino, A., Dolphin, T., Medina-Lopez, E., 2022. Multispectral satellite imagery and machine learning for the extraction of shoreline indicators. Coast. Eng. 174, 104102. https://doi.org/10.1016/j.coastaleng.2022.104102

Merchant, M.A., 2020. Classifying open water features using optical satellite imagery and an object-oriented convolutional neural network. Remote Sens. Lett. 11, 1127–1136. https://doi.org/10.1080/2150704X.2020.1825869

Millard, K., Richardson, M., 2015. On the Importance of Training Data Sample Selection in Random Forest Image Classification: A Case Study in Peatland Ecosystem Mapping. Remote Sens. 7, 8489–8515. https://doi.org/10.3390/rs70708489

Mollick, T., Azam, M.G., Karim, S., 2023. Geospatial-based machine learning techniques for land use and land cover mapping using a high-resolution unmanned aerial vehicle image. Remote Sens. Appl. Soc. Environ. 29, 100859. https://doi.org/10.1016/j.rsase.2022.100859

Niculescu, S., Billey, A., Jr, H.T.-O.-A., 2018. Random forest classification using Sentinel-1 and Sentinel-2 series for vegetation monitoring in the Pays de Brest (France), in: Remote Sensing for Agriculture, Ecosystems, and Hydrology XX. Presented at the Remote Sensing for Agriculture, Ecosystems, and Hydrology XX, SPIE, p. 1078305. https://doi.org/10.1117/12.2325546

Paskoff, R., 1984. Rapport III. 7 Erosion et protection des plages : une nouvelle approche 1–7.

Puissant, A., Rougier, S., Stumpf, A., 2014. Object-oriented mapping of urban trees using Random Forest classifiers. Int. J. Appl. Earth Obs. Geoinformation 26, 235–245. https://doi.org/10.1016/j.jag.2013.07.002

Ramesh, V., Singh, D., 2020. Monitoring Shorelines via High-Resolution Satellite Imagery and Deep Learning.

Rodriguez-Galiano, V.F., Ghimire, B., Rogan, J., Chica-Olmo, M., Rigol-Sanchez, J.P., 2012. An assessment of the effectiveness of a random forest classifier for land-cover classification. ISPRS J. Photogramm. Remote Sens. 67, 93–104. https://doi.org/10.1016/j.isprsjprs.2011.11.002

Roy, S., Mahapatra, M., Chakraborty, A., 2018. Shoreline change detection along the coast of Odisha, India using digital shoreline analysis system. Spat. Inf. Res. 26, 563–571. https://doi.org/10.1007/s41324-018-0199-6

Sabat-Tomala, A., Raczko, E., Zagajewski, B., 2020. Comparison of Support Vector Machine and Random Forest Algorithms for Invasive and Expansive Species Classification Using Airborne Hyperspectral Data. Remote Sens. 12, 516. https://doi.org/10.3390/rs12030516

Sanlaville, P., 2001. Roland Paskoff - L’élévation du niveau de la mer et les espaces côtiers. Le mythe et la réalité 3.

Seale, C., Redfern, T., Chatfield, P., Luo, C., Dempsey, K., 2022. Coastline detection in satellite imagery: A deep learning approach on new benchmark data. Remote Sens. Environ. 278, 113044. https://doi.org/10.1016/j.rse.2022.113044

Serbaji, M.M., Bouaziz, M., Weslati, O., 2023. Soil Water Erosion Modeling in Tunisia Using RUSLE and GIS Integrated Approaches and Geospatial Data. Land 12, 548. https://doi.org/10.3390/land12030548

Sertel, E., Ekim, B., Ettehadi Osgouei, P., Kabadayi, M.E., 2022. Land Use and Land Cover Mapping Using Deep Learning Based Segmentation Approaches and VHR Worldview-3 Images. Remote Sens. 14, 4558. https://doi.org/10.3390/rs14184558

Shayeganpour, S., Tangestani, M.H., Homayouni, S., Vincent, R.K., 2021. Evaluating pixel-based vs. object-based image analysis approaches for lithological discrimination using VNIR data of WorldView-3. Front. Earth Sci. 15, 38–53. https://doi.org/10.1007/s11707-020-0848-7

Šiljeg, A., Panđa, L., Domazetović, F., 2022. Comparative Assessment of Pixel and Object-Based Approaches for Mapping of Olive Tree Crowns Based on UAV Multispectral Imagery.

Souto-Ceccon, P., Simarro, G., Ciavola, P., Taramelli, A., Armaroli, C., 2023. Shoreline Detection from PRISMA Hyperspectral Remotely-Sensed Images. Remote Sens. 15, 2117. https://doi.org/10.3390/rs15082117

Sreekesh, S., Kaur, N., Sreerama Naik, S.R., 2020. An OBIA and Rule Algorithm for Coastline Extraction from High- and Medium-Resolution Multispectral Remote Sensing Images. Remote Sens. Earth Syst. Sci. 3, 24–34. https://doi.org/10.1007/s41976-020-00032-z

Sunder, S., Ramsankaran, R., Ramakrishnan, B., 2017. Inter-comparison of remote sensing sensing-based shoreline mapping techniques at different coastal stretches of India. Environ. Monit. Assess. 189, 290. https://doi.org/10.1007/s10661-017-5996-1

Toure, S., Diop, O., Kpalma, K., Maiga, A., 2019. Shoreline Detection using Optical Remote Sensing: A Review. ISPRS Int. J. Geo-Inf. 8, 75. https://doi.org/10.3390/ijgi8020075

Tsiakos, C.-A.D., Chalkias, C., 2023. Use of Machine Learning and Remote Sensing Techniques for Shoreline Monitoring: A Review of Recent Literature. Appl. Sci. 13, 3268. https://doi.org/10.3390/app13053268

Valderrama-Landeros, L., Flores-de-Santiago, F., 2019. Assessing coastal erosion and accretion trends along two contrasting subtropical rivers based on remote sensing data. Ocean Coast. Manag. 169, 58–67. https://doi.org/10.1016/j.ocecoaman.2018.12.006

Varo-Martínez, M.Á., Navarro-Cerrillo, R.M., 2021. Stand Delineation of Pinus sylvestris L. Plantations Suffering Decline Processes Based on Biophysical Tree Crown Variables: A Necessary Tool for Adaptive Silviculture. Remote Sens. 13, 436. https://doi.org/10.3390/rs13030436

Wang, J., Wang, L., Feng, S., Peng, B., Huang, L., Fatholahi, S.N., Tang, L., Li, J., 2023. An Overview of Shoreline Mapping by Using Airborne LiDAR. Remote Sens. 15, 253. https://doi.org/10.3390/rs15010253

Wang, Z., Liu, J., Li, J., Zhang, D., 2018. Multi-Spectral Water Index (MuWI): A Native 10-m Multi-Spectral Water Index for Accurate Water Mapping on Sentinel-2. Remote Sens. 10, 1643. https://doi.org/10.3390/rs10101643

Wicaksono, A., Wicaksono, P., 2019. Geometric Accuracy Assessment for Shoreline Derived from NDWI, MNDWI, and AWEI Transformation on Various Coastal Physical Typology in Jepara Regency using Landsat 8 OLI Imagery in 2018. Geoplanning J. Geomat. Plan. 6, 55. https://doi.org/10.14710/geoplanning.6.1.55-72

Yan, D., Yao, X., Li, J., Qi, L., Luan, Z., 2021. Shoreline Change Detection and Forecast along the Yancheng Coast Using a Digital Shoreline Analysis System. Wetlands 41, 47. https://doi.org/10.1007/s13157-021-01444-3

Yan, Y., 2023. Inversion et assimilation de données de télédétection: Estimation des paramètres géophysiques. ISTE Group.

Yang, M., Zou, L., Cai, H., Qiang, Y., Lin, B., Zhou, B., Abedin, J., Mandal, D., 2022. Spatial–Temporal Land Loss Modeling and Simulation in a Vulnerable Coast: A Case Study in Coastal Louisiana. Remote Sens. 14, 896. https://doi.org/10.3390/rs14040896

Yang, X., Qin, Q., Yésou, H., Ledauphin, T., Koehl, M., Grussenmeyer, P., Zhu, Z., 2020. Monthly estimation of the surface water extent in France at a 10-m resolution using Sentinel-2 data. Remote Sens. Environ. 244, 111803. https://doi.org/10.1016/j.rse.2020.111803

Zaabar, N., Niculescu, S., Kamel, M.M., 2022. Application of Convolutional Neural Networks With Object-Based Image Analysis for Land Cover and Land Use Mapping in Coastal Areas: A Case Study in Ain Témouchent, Algeria. IEEE J. Sel. Top. Appl. Earth Obs. Remote Sens. 15, 5177–5189. https://doi.org/10.1109/JSTARS.2022.3185185

Zagórski, P., Jarosz, K., Superson, J., 2020. Integrated Assessment of Shoreline Change along the Calypsostranda (Svalbard) from Remote Sensing, Field Survey and GIS. Mar. Geod. 43, 433–471. https://doi.org/10.1080/01490419.2020.1715516

Zhang, Liangpei, Zhang, Lefei, Du, B., 2016. Deep Learning for Remote Sensing Data: A Technical Tutorial on the State of the Art. IEEE Geosci. Remote Sens. Mag. 4, 22–40. https://doi.org/10.1109/MGRS.2016.2540798

Zhao, B., Liu, Yongxue, Wang, L., Liu, Yongchao, Sun, C., Fagherazzi, S., 2022. Stability evaluation of tidal flats based on time-series satellite images: A case study of the Jiangsu central coast, China. Estuar. Coast. Shelf Sci. 264, 107697. https://doi.org/10.1016/j.ecss.2021.107697

Zhu, X.X., Tuia, D., Mou, L., Xia, G.-S., Zhang, L., Xu, F., Fraundorfer, F., 2017. Deep Learning in Remote Sensing: A Comprehensive Review and List of Resources. IEEE Geosci. Remote Sens. Mag. 5, 8–36. https://doi.org/10.1109/MGRS.2017.2762307